Draft version September 15, 2015
Preprint typeset using LaTeX style emulateapj v. 5/2/11

ADIABATIC BLACK HOLE GROWTH IN SÉRSIC MODELS OF ELLIPTICAL GALAXIES

Naveen Jingade[1,2], Tarun Deep Saini[1] and Scott Tremaine[3]

Draft version September 15, 2015

ABSTRACT

We have examined the effect of slow growth of a central black hole on spherical galaxies that obey Sérsic or $R^{1/m}$ surface-brightness profiles. During such growth the actions of each stellar orbit are conserved, which allows us to compute the final distribution function if we assume that the initial distribution function is isotropic. We find that black-hole growth leads to a central cusp or "excess light", in which the surface brightness varies with radius as $R^{-1.3}$ (with a weak dependence on Sérsic index m), the line-of-sight velocity dispersion varies as $R^{-1/2}$, and the velocity anisotropy is $\beta \simeq -0.24$ to -0.28 depending on m. The excess stellar mass in the cusp scales approximately linearly with the black-hole mass, and is typically 0.5–0.85 times the black-hole mass. This process may strongly influence the structure of nuclear star clusters if they contain black holes.

1. INTRODUCTION

Most elliptical galaxies have surface-brightness profiles that are fit well by the empirical Sérsic formula, given by equation (1), with Sérsic index m varying from 2 to much larger values (Kormendy et al. 2009). In addition to the index m, the Sérsic formula has just two parameters: I_0 is the central surface brightness and R_e is the effective radius, the projected radius containing half of the total luminosity.

It has been observed (Kormendy et al. 2009) that the Sérsic profile fits elliptical galaxies over a wide range of radii, but there are often deviations from the fitting formula at small radii. These deviations are of two kinds: either "missing light" or "excess light" near the centers compared to the inward extrapolation of the Sérsic profile. Missing-light or "core" ellipticals generally have higher luminosities ($M_V \lesssim -21.7$) than excess-light ellipticals ($M_V \gtrsim -21.5$). Figures 1 and 2, taken from Kormendy et al. (2009), show the surface-brightness profiles of an excess-light and a missing-light elliptical galaxy.

The formation of a core is generally attributed to the dynamical excitation of stellar orbits due to a binary black hole (hereafter BH), although there is little or no direct evidence for this hypothesis. Excess light is generally attributed to late star formation from gas that has become concentrated near the galaxy center. The division of ellipticals into these two classes, and the explanations given above for this dichotomy, date back at least to Faber et al. (1997).

Most elliptical galaxies appear to have massive BHs at their centers. In this work we assume that these BHs form slowly by the accretion of gas from larger radii. In this case the surrounding stellar system will contract as the central mass grows, because the stellar orbits conserve their adiabatic invariants or actions. If the galaxy began with a Sérsic surface-brightness profile, this process will naturally produce excess light relative to the Sérsic profile near the center of the galaxy, and the corresponding excess stellar mass will be simply related to the mass of the BH and the properties of the initial Sérsic profile. The main goal of the paper is to work out these relations and to compare the predictions of this simple model to the observations.

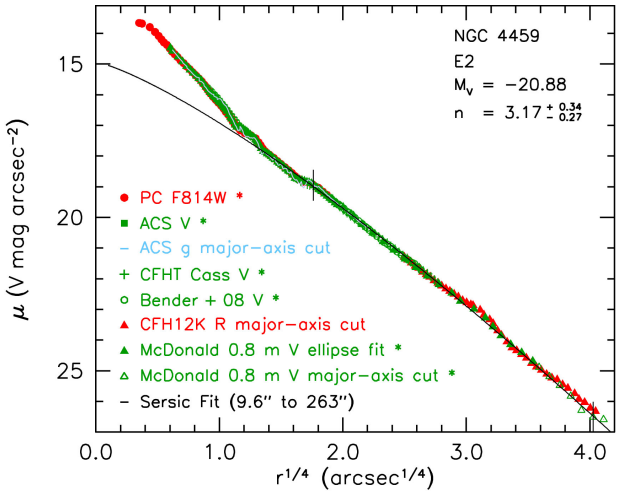

FIG. 1.— Surface-brightness profile of the dwarf galaxy NGC 4459, an excess-light elliptical. The curve shows the best-fitting Sérsic profile, with index $m = 3.17$ (Kormendy et al. 2009). Reproduced by permission of the AAS.

Pioneering studies of this process were carried out by Peebles (1972) and Young (1980). These studies assumed that the galaxies were spherical, as do we, but in contrast they assumed that the stellar distribution function (DF) near the center of the galaxy was Maxwellian before the formation of the BH. They found that as the BH grew the stellar DF developed a cusp in which the density varied as $\rho \sim r^{-3/2}$, corresponding to a surface brightness $I(R) \sim R^{-1/2}$. However, a Sérsic profile does not have a Maxwellian DF, and the properties of the cusp formed by

naveen@rri.res.in, tarun@physics.iisc.ernet.in
tremaine@ias.edu
[1] Department of Physics, Indian Institute of Science, Bangalore 560 012, India
[2] A & A, Raman Research Institute, Bangalore 560080, India
[3] Institute for Advanced Study, Princeton, NJ 08540, USA

the adiabatic growth of a central BH depend strongly on the DF (Quinlan et al. 1995). In general we expect (and shall find) the cusp formed in an initial Sérsic model to be steeper than the one found by Peebles and Young.

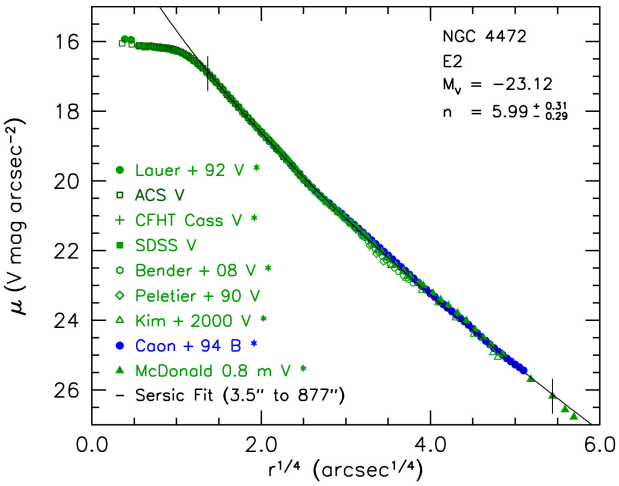

FIG. 2.— Surface-brightness profile of the giant galaxy NGC 4472, a missing-light elliptical. The curve shows the best-fitting Sérsic profile, with index $m = 5.99$ (Kormendy et al. 2009). Reproduced by permission of the AAS.

In §2 we review the properties of Sérsic models and derive the dynamical quantities of interest (density, potential, DF, velocity moments) assuming spherical symmetry, constant mass-to-light ratio Υ, and isotropic velocity dispersion. We then slowly add a central point mass representing the BH and evolve the system under the assumption of adiabatic invariance of the stellar orbits. The numerical methods are described in §3. The surface-brightness distribution, anisotropy parameter, excess mass, and line-of-sight velocity-dispersion distribution of the adiabatic models are described in §§4 and 5, and the observations in §6. The conclusions are in §7.

2. INITIAL SET UP

2.1. *Density*

The surface-brightness distribution of a spherical galaxy is modeled well by the Sérsic law (Sérsic 1963; Sérsic 1968; Ciotti 1991)

$$I(\eta) = I_0 \exp(-b\,\eta^{1/m}) \quad \text{where} \quad \eta = R/R_e \qquad (1)$$

and m is the Sérsic index. Here R_e is the effective radius, the radius on the sky that contains half the total light. This definition of R_e requires that the parameter b is given by

$$2\,\gamma(2m, b) = \Gamma(2m) \qquad (2)$$

where γ is the incomplete gamma function. The function $b(m)$ is well fitted by the linear interpolation $b(m) = 2m - 0.324$, with relative error less than 0.001 for $0.5 < m < 10$ (Ciotti 1991). The exact values of $b(m)$ for several values of m are given in Table 1. As $m \to \infty$, $b/m \to 2$ and $I(R) \sim R^{-2}$ over a wide range of radii around R_e.

The luminosity density for given surface brightness $I(R)$ can be obtained by the Abel integral

$$j(r) = -\frac{1}{\pi}\int_r^\infty \frac{\mathrm{d}R}{\sqrt{R^2 - r^2}}\frac{\mathrm{d}I}{\mathrm{d}R}. \qquad (3)$$

If we assume that the galaxy has constant mass-to-light ratio Υ, then its mass density $\rho(r) = \Upsilon j(r)$. Substituting equation (1) in equation (3) and introducing the dimensionless radius $s = r/R_e$, we get

$$\rho_m(s) = \Upsilon\frac{I_0}{R_e}\widetilde{\rho}_m(s) = \frac{\Sigma_0}{R_e}\widetilde{\rho}_m(s) \quad \text{where} \quad \Sigma_0 = \Upsilon\, I_0,$$
$$\widetilde{\rho}_m(s) = \frac{b}{\pi\, m s^{(m-1)/m}}\int_0^1 \frac{\exp[-b(s/x)^{1/m}]}{x^{1/m}}\frac{\mathrm{d}x}{\sqrt{1-x^2}} \qquad (4)$$

where $x = s/\eta$. For $m > 1$ the dimensionless density $\widetilde{\rho}_m(s)$ diverges at the origin as

$$\widetilde{\rho}_m(s) \sim \frac{b}{2\pi m}\frac{1}{s^{(m-1)/m}} B\left[\tfrac{1}{2}, \tfrac{1}{2}(1 - 1/m)\right] \qquad (5)$$

where B is the beta function. The dimensionless density $\widetilde{\rho}_m(s)$ is plotted in Figure 3 for several values of m.

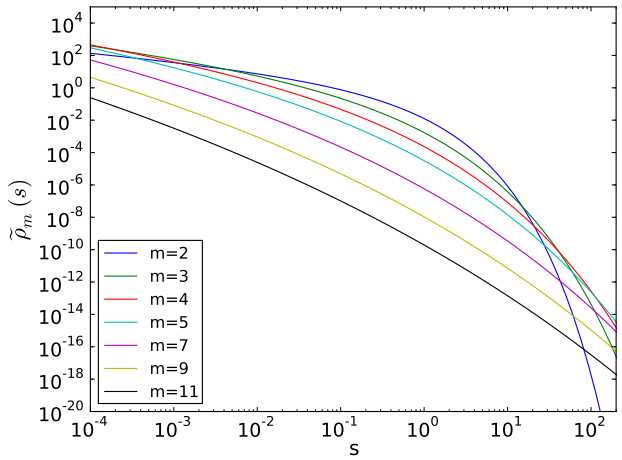

FIG. 3.— The dimensionless density $\widetilde{\rho}_m(s)$ (eq. 4) for $2 \le m \le 11$. Here $s = r/R_e$, the ratio of the radius to the effective radius.

2.2. *Potential*

The potential is obtained by solving the Poisson equation

$$\nabla^2\Phi = \frac{1}{r^2}\frac{\mathrm{d}}{\mathrm{d}r}\left(r^2\frac{\mathrm{d}\Phi}{\mathrm{d}r}\right) = 4\pi G\rho. \qquad (6)$$

If we define $\Phi_m(r) = 4\pi G\,\Sigma_0 R_e \widetilde{\Phi}_m(s)$, then in dimensionless variables we have

$$\frac{1}{s^2}\frac{\mathrm{d}}{\mathrm{d}s}\left(s^2\frac{\mathrm{d}\widetilde{\Phi}_m}{\mathrm{d}s}\right) = \widetilde{\rho}_m. \qquad (7)$$

In integral form,

$$\widetilde{\Phi}_m(s) = -\int_s^\infty \frac{\widetilde{M}_m(s')}{s'^2}\mathrm{d}s' \quad \text{where}$$
$$\widetilde{M}_m(s) = \int_0^s \widetilde{\rho}_m(s')s'^2\,\mathrm{d}s' \qquad (8)$$

is the mass of the system measured in units of $4\pi\,\Sigma_0 R_e^2$. One cannot solve the integral in general for the density given by equation (4) but we can obtain the central potential (Ciotti 1991), which is useful in what follows:

$$\Phi(0) = -4G\Upsilon \int_0^\infty \mathrm{d}R\, I(R) = -4\pi G \int_0^\infty r\,\rho(r)\,\mathrm{d}r \quad (9)$$

from which the dimensionless central potential is found to be:

$$\widetilde{\Phi}_m(0) = -\frac{\Gamma(m+1)}{\pi b^m}. \quad (10)$$

Thus the central potential is finite even though the density diverges at the center for $m > 1$. The values of the dimensionless central potential and dimensionless mass for several values of the Sérsic index m are given in Table 1.

Poisson's equation (7) has to be solved numerically with the initial condition (10), taking $\mathrm{d}\widetilde{\Phi}_m/\mathrm{d}s = 0$ at $s = 0$. Plots of the potential for different values of m are shown in Figure 4.

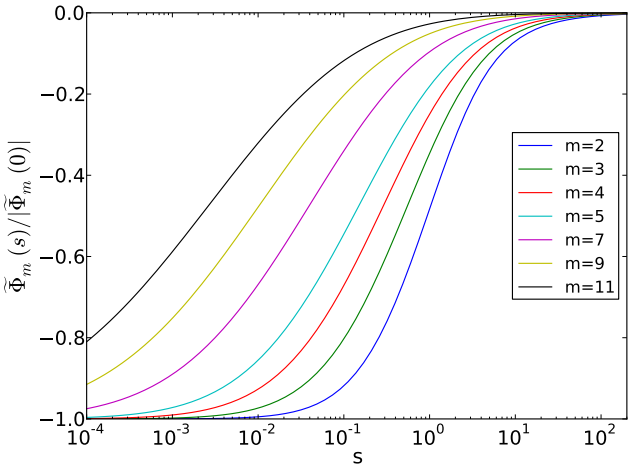

FIG. 4.— The normalized potential $\widetilde{\Phi}_m(s)/|\widetilde{\Phi}_m(0)|$ (eqs. 8 and 10) for $2 \le m \le 11$. Here $s = r/R_e$, the ratio of the radius to the effective radius.

TABLE 1
THE DIMENSIONLESS PARAMETERS b, $|\widetilde{\Phi}_m(0)|$ AND $\widetilde{M}_m$ FOR DIFFERENT VALUES OF THE SÉRSIC INDEX m.

m	b	$\lvert\widetilde{\Phi}_m(0)\rvert$	$\widetilde{M}_m$
2	3.67	4.17×10^{-2}	2.91×10^{-2}
3	5.67	1.04×10^{-2}	5.41×10^{-3}
4	7.66	2.21×10^{-3}	8.42×10^{-4}
5	9.66	4.52×10^{-4}	1.27×10^{-4}
7	13.66	1.80×10^{-5}	2.74×10^{-5}
9	17.66	6.88×10^{-7}	5.68×10^{-8}
11	21.66	2.57×10^{-8}	1.17×10^{-9}

2.3. *Distribution function*

We shall assume for simplicity that the initial phase-space DF of the stars in the galaxy is ergodic, that is, the velocity distribution is isotropic at every point in space and the DF depends only on the energy E. In such a case, the DF can be calculated from the known density and potential of the galaxy as follows:

$$f(E) = \frac{1}{\sqrt{8}\,\pi^2} \int_E^0 \frac{\mathrm{d}\Phi}{\sqrt{\Phi - E}} \frac{\mathrm{d}^2\rho}{\mathrm{d}\Phi^2}. \quad (11)$$

Using the dimensionless potential and density, we can write the DF in dimensionless form as

$$f_m(E) = \frac{1}{(4\pi G)^{3/2}(\Sigma_0 R_e^5)^{1/2}}\,\widetilde{f}_m(\widetilde{E}) \qquad \text{where}$$

$$\widetilde{f}_m(\widetilde{E}) = \frac{1}{\sqrt{8}\,\pi^2} \int_{\widetilde{E}}^0 \frac{\mathrm{d}\widetilde{\Phi}}{\sqrt{\widetilde{\Phi} - \widetilde{E}}} \frac{\mathrm{d}^2\widetilde{\rho}_m}{\mathrm{d}\widetilde{\Phi}^2}. \quad (12)$$

The DF is plotted for various values of m in Figure 5. One can see that for all values of m the DF is positive, and that it diverges as $E \to \Phi(0)$; it is straightforward to show that

$$\widetilde{f}_m(\widetilde{E}) \sim \left[\widetilde{E} - \widetilde{\Phi}_m(0)\right]^{-\alpha}, \qquad \alpha = \frac{5m+1}{2(m+1)}. \quad (13)$$

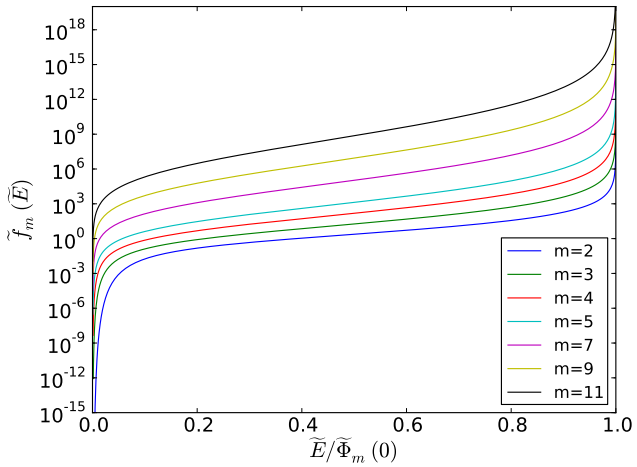

FIG. 5.— The DF $\widetilde{f}_m(\widetilde{E})$ as a function of normalized energy $\widetilde{E}/\widetilde{\Phi}_m(0)$ for $2 \le m \le 11$.

2.4. *Velocity moments*

For the remainder of this paper we will drop the tildes on E, Φ, ρ, etc., and it should be understood that these quantities are dimensionless. According to Jeans's theorem, a stationary spherical DF can only depend on the energy $E = \frac{1}{2}v_r^2 + \frac{1}{2}v_t^2 + \Phi(s)$ and the angular momentum $L = s\,v_t$, where v_r and v_t are the radial and tangential velocities. We can obtain the density, and the radial and tangential velocity dispersions for this DF as

$$\rho(s) = 4\pi \int_{\Phi(s)}^{0} \mathrm{d}E\,[2(E-\Phi)]^{1/2} \int_0^1 \frac{\mathrm{d}y\, y\, f(E, L_{\max}\, y)}{\sqrt{1-y^2}}, \tag{14}$$

$$\overline{v_r^2}(s) = \frac{4\pi}{\rho(s)} \int_{\Phi(s)}^{0} \mathrm{d}E\,[2(E-\Phi)]^{3/2} \int_0^1 \mathrm{d}y\, y\, \sqrt{1-y^2}\, f(E, L_{\max}\, y), \tag{15}$$

$$\overline{v_t^2}(s) = \frac{4\pi}{\rho(s)} \int_{\Phi(s)}^{0} \mathrm{d}E\,[2(E-\Phi)]^{3/2} \int_0^1 \frac{\mathrm{d}y\, y^3\, f(E, L_{\max}\, y)}{\sqrt{1-y^2}}, \tag{16}$$

where

$$L_{\max}(E,s) = \{2\,s^2[E-\Phi(s)]\}^{1/2}, \quad y = L/L_{\max}; \tag{17}$$

$L_{\max}$ is the maximum angular momentum for an orbit of energy E that passes through radius s. Note that the velocity dispersions in the θ and ϕ directions are $\overline{v_\phi^2} = \overline{v_\theta^2} = \frac{1}{2}\overline{v_t^2}$. For numerical work, the inner integral over y can be evaluated using Gauss–Chebyshev quadrature and the outer integral over E by Gauss–Legendre quadrature.

We then project the density and velocity moments on the plane of sky to obtain the surface density

$$\Sigma(\eta) = 2\int_\eta^\infty \frac{s\,\rho(s)\,\mathrm{d}s}{\sqrt{s^2-\eta^2}} \tag{18}$$

and the line-of-sight velocity dispersion

$$\sigma_{||}^2(\eta) = \frac{2}{\Sigma(\eta)} \int_\eta^\infty \frac{s\,\rho(s)\,\mathrm{d}s}{\sqrt{s^2-\eta^2}} \left[\left(1-\frac{\eta^2}{s^2}\right)\overline{v_r^2} + \frac{\eta^2}{2\,s^2}\,\overline{v_t^2}\right]. \tag{19}$$

The anisotropy parameter is

$$\beta(s) = 1 - \frac{\overline{v_t^2}(s)}{2\,\overline{v_r^2}(s)} \tag{20}$$

which is 0 for an isotropic velocity distribution, $-\infty$ for circular orbits and $+1$ for radial orbits.

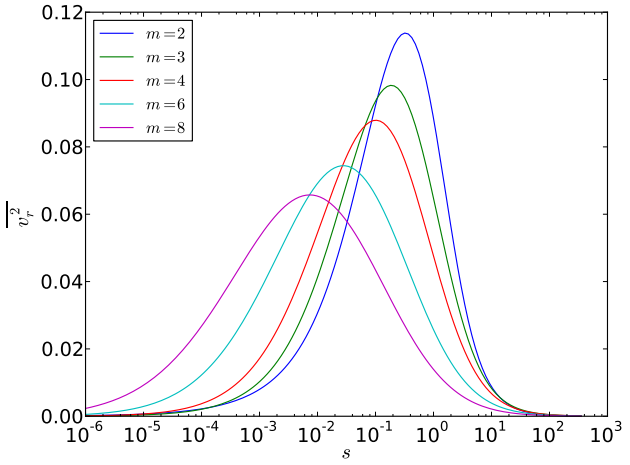

FIG. 6.— The initial isotropic velocity dispersion of the galaxy for varying Sérsic index m.

The initial Sérsic models are ergodic, so the velocity distribution is isotropic, $\beta = 0$, and the DF depends only on energy, not angular momentum. The velocity dispersion $\overline{v_r^2}(s) = \frac{1}{2}\overline{v_t^2}(s)$ is shown in Figure 6.

2.5. *Actions*

The radial and azimuthal actions are

$$I_r = 2\int_{s_-}^{s_+} \sqrt{2[E-\Phi(s)] - L^2/s^2}\,\mathrm{d}s \qquad I_t = 2\,\pi\,L, \tag{21}$$

where s_- and s_+ are the pericenter and apocenter distances of the orbit, given implicitly by

$$2\,s_\pm^2[E-\Phi(s_\pm)] - L^2 = 0. \tag{22}$$

Since actions are conserved during the adiabatic growth of the central BH, the DF is also conserved at each point in action space. In terms of energy and angular momentum, a star that is initially at (E, L) in phase space when the potential is $\Phi(s)$ will move to a new phase point (E^*, L) when the potential changes to $\Phi^*(s)$. By equating the initial and final actions, we find the relation $E = E(E^*, L)$. Then the new DF $f^*(E^*, L)$ is related to the original DF $f(E, L)$ by $f^*(E^*, L) = f[E(E^*, L), L]$.

3. NUMERICAL METHODS

The density, DF, potential and other galaxy properties are evaluated on a grid: $\rho_i = \rho(s_i)$, $\Phi_i = \Phi(s_i)$, $f_{jk} = f(E_j, L_k)$, and so on. The radial grid is equally spaced in $\log(s)$ with roughly 200 points between $s_{\min} = 10^{-6}$ and $s_{\max} = 2 \times 10^2$. The energy grid points E_j are chosen to match the potential Φ_i at the radial grid points; since $\Phi(r)$ varies as the BH grows, the locations of the energy grid points E_j also vary. The grid points for angular momentum are spaced uniformly between $x = 0$ and $x = 1$ where $x = L/L_c(E)$ and $L_c(E)$ is the angular momentum of a circular orbit at the given energy. Typically we use 200 grid points in energy and 20 in angular momentum.

Following Young (1980), the program executes the following steps for a given Sérsic index m:

1. The density $\rho_i = \rho(s_i)$ is obtained from equation (4) at all points on the radial grid (recall that we have dropped the tildes on all dimensionless quantities).

2. The gravitational potential $\Phi_i = \Phi(s_i)$ is obtained from Poisson's equation (8) at all points on the grid.

3. The initial DF $f_{jk} = f(E_j)$ is obtained from ρ_i and Φ_i using equation (12). The initial values f_{jk} are independent of the angular momentum $x_k\, L_c(E_j)$ since the initial DF is ergodic.

4. The radial action $I_{jk} = I_r(E_j, x_k)$ is calculated for the potential $\Phi(s)$ at each point on the energy-angular momentum grid $[E_j, x_k\, L_c(E_j)]$, using equation (21).

5. A BH of mass $M_\bullet$ is added at the center of the galaxy, thereby modifying the potential to $\Phi^*(s) = \Phi(s) - M_\bullet/s$.

6. In this new potential we compute the angular momentum of circular orbits as a function of energy, $L_c^*(E^*)$.

7. A new energy-angular momentum grid $[E_j^*, x_k\, L_c^*(E_j^*)]$ is defined, in which the new energies E_j^* match the new potentials $\Phi_j^* = \Phi^*(s_j)$ at the radial grid points. The new action $I_{jk}^* = I_r^*(E_j^*, x_k)$ is computed on the new energy-angular momentum grid $[E_j^*, x_k\, L_c^*(E_j^*)]$.

8. Since actions are conserved, a star at (E, x) evolves during the growth of the BH to (E^*, x^*) where $I_r^*(E^*, x^*) = I_r(E, x)$, $x^*\, L_c^*(E^*) = x\, L_c(E)$. We solve for the original (E, x) at each point on the new energy-angular momentum grid $[E_j^*, x_k\, L_c^*(E_j^*)]$ and then compute the new DF as $f^*(E^*, x^* L_c^*) = f[E(E^*, x^* L_c^*)]$.

9. Using the DF f^* and potential Φ^* we compute the resulting density ρ^{**} from equation (14) and the potential Φ^{**} from Poisson's equation (8). We then replace ρ^* and Φ^* by ρ^{**} and Φ^{**} and return to step 6.

After about 20 iterations this algorithm converges, yielding a DF for the stellar system from which quantities of interest like density, surface brightness profile, and velocity dispersion can be computed.

4. EXCESS MASS

We wish to quantify the excess light or stellar mass accumulated near the center of the galaxy as the result of the adiabatic adjustment of the stellar orbits to the growth of the BH. Since the excess has appeared at the center only because of the rearrangement of the stars, the total luminosity of the galaxy is unchanged: the density goes up substantially close to the center, and decreases by a much smaller amount at large radii. The definition of "excess mass" is therefore somewhat arbitrary, but most reasonable definitions will give very similar values. We define the"cross-over radius" as the value of the dimensionless radius $\eta = R/R_e$ at which the initial and final surface-density profiles cross (see Figure 7). Let $\Sigma(\eta)$ and $\Sigma^*(\eta)$ be the dimensionless initial and final surface-density profiles, then η_c is defined by the equality $\Sigma^*(\eta_c) = \Sigma(\eta_c)$;

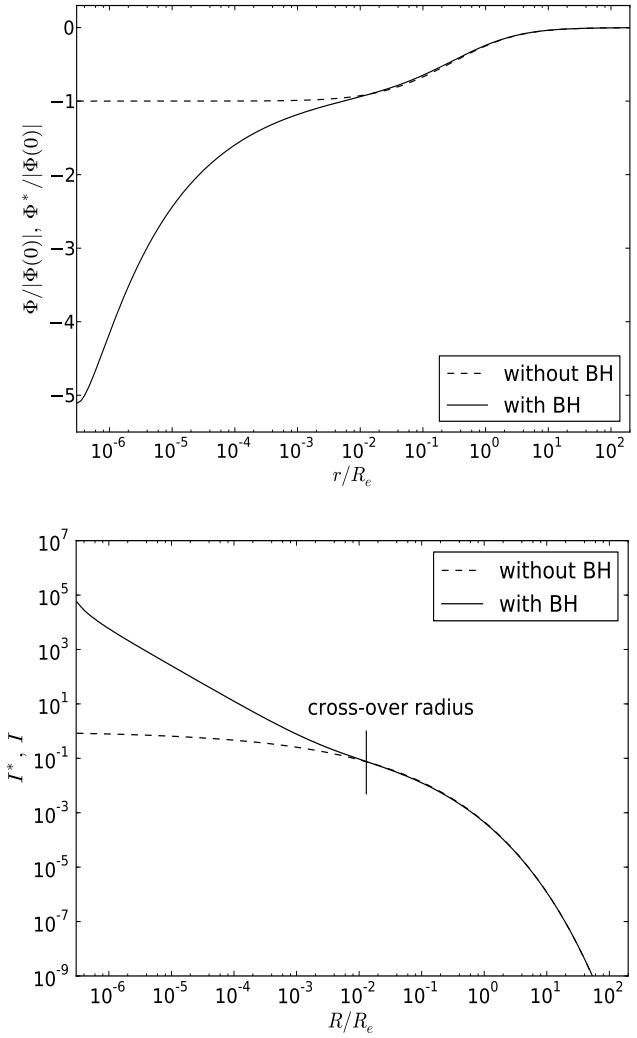

FIG. 7.— Typical potential and surface density of a galaxy with and without a BH. The Sérsic index $m = 4$ and the black-hole mass relative to the galaxy mass is $M_\bullet/M_G = 1.877 \times 10^{-3}$.

we have verified that this solution exists and is unique. The excess mass is defined as

$$M_e = \tfrac{1}{2} \int_0^{\eta_c} \eta[\Sigma^*(\eta) - \Sigma(\eta)]\, \mathrm{d}\eta\,. \qquad (23)$$

The factor $\frac{1}{2}$ appears in the above equation so that the dimensional definition of the excess mass is $M_e = 2\pi \int_0^{R_c} [\Sigma^*(R) - \Sigma(R)] R\, \mathrm{d}R$ (cf. eq. 8)—in other words it arises because the volume element is $4\pi s^2\, \mathrm{d}s$ but the area element is $2\pi\eta\, \mathrm{d}\eta$.

5. RESULTS AND DISCUSSION

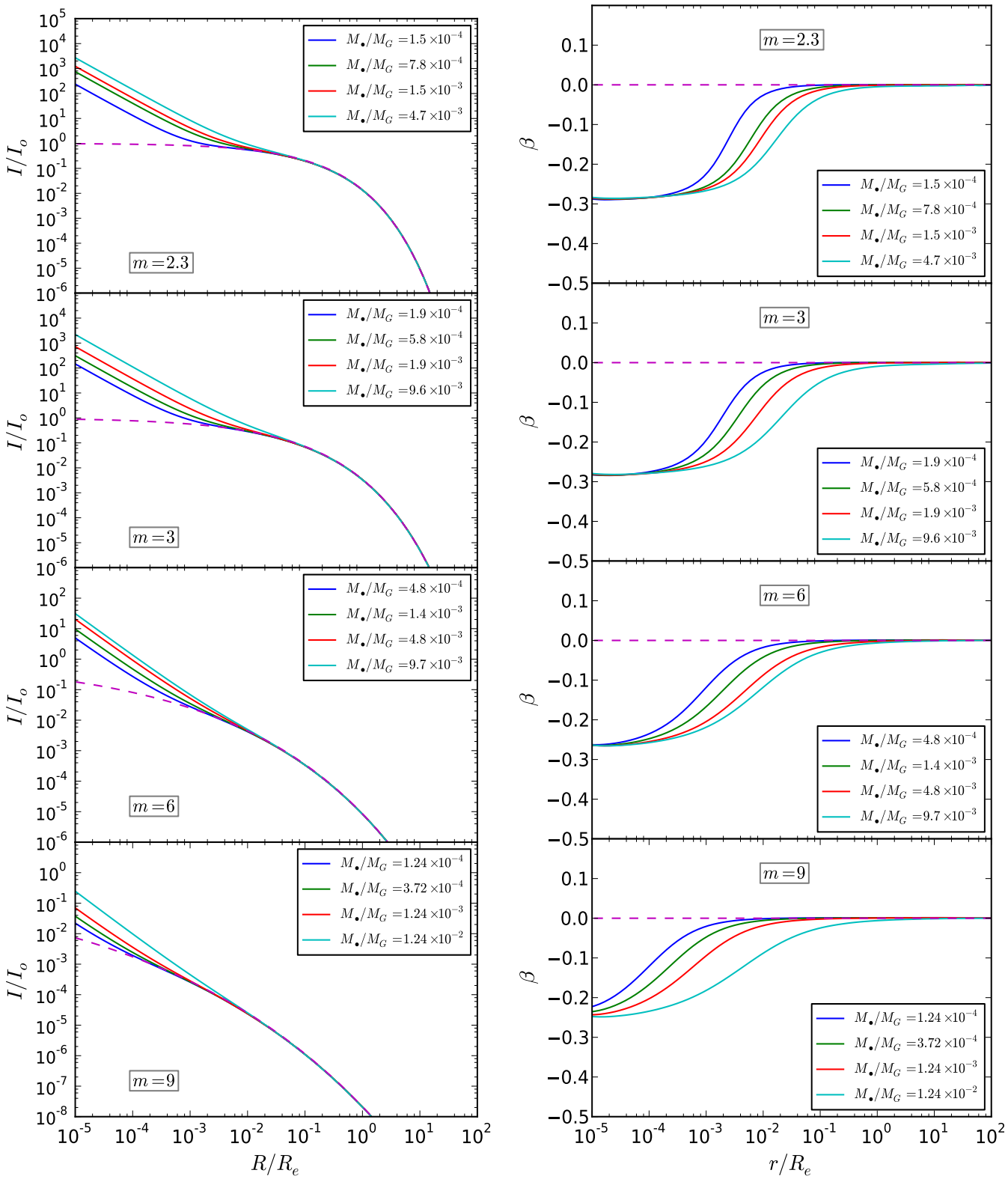

FIG. 8.— Surface-brightness profile (left) and anisotropy parameter (right) after the adiabatic growth of a BH in a galaxy with Sérsic index $m = 2.3$, $m = 3$, $m = 6$, and $m = 9$.

The surface-brightness profile $I(R)$ and anisotropy parameter $\beta(r)$ are plotted in Figure 8 for Sérsic index $m = 2.3$, 3, 6 and 9 for dimensionless BH masses varying from 10^{-5} to 5×10^{-3}. The BH masses are chosen such that they are 10^{-4} to few times 10^{-2} of the galaxy mass (M_G).

5.1. *Surface-density cusp*

The prominence of the surface-brightness or surface-density cusps shown in Figure 8 varies with the Sérsic index m. For smaller m the cusp is more prominent, partly because the initial surface-brightness profile near the center is flatter. For large m, even with the largest BH masses, the cusp caused by the BH is hardly noticeable (see $m = 9$ case in Figure 8).

One can derive the approximate behavior of the surface-density cusp analytically (Quinlan et al. 1995; Gondolo & Silk 1999)

$$\rho^* \sim r^{-\Gamma}, \quad \Sigma^* \sim R^{1-\Gamma}, \quad \Gamma = 2 + \frac{1}{4-\gamma} = \frac{7m+2}{3m+1}. \tag{24}$$

where $\gamma = (m-1)/m$ is the exponent of the initial cusp (see eq. 5). For the Sérsic index $m = 2.3$, $\rho^* \sim r^{-2.29}$ and $\Sigma^* \sim R^{-1.29}$ and for $m = 9$, $\rho^* \sim r^{-2.32}$ and $\Sigma^* \sim R^{-1.32}$. We see that the exponent of the central surface-density cusp does not vary strongly with Sérsic index. Thus the cusp becomes less prominent as m increases and the initial profile becomes more cuspy.

5.2. *Anisotropy and velocity cusp*

The line-of-sight velocity dispersion (eq. 19) is shown in Figure 9. Both the radial and tangential dispersions $\overline{v_r^2}$ and $\overline{v_t^2}$ scale as r^{-1} near the BH and this scaling is evident in Figure 9. In contrast, the velocity dispersion goes to zero at the center for all values of the Sérsic index m for a galaxy without a central BH.

The anisotropy parameter β is plotted for $m = 2.3$ to $m = 9$ in Figure 8. The plots show that as a result of the BH growth the stellar DF develops a tangential anisotropy $-\beta \simeq 0.24$–0.28 near the center. The anisotropy depends only weakly on the Sérsic index, and is independent of the BH mass: as the BH mass grows the anisotropy simply extends to larger distances.

Using an approximate expression for the radial action near the center of a Sérsic model due to Gondolo & Silk (1999), we compute in the Appendix the ratio of the radial and tangential velocity dispersions and thus the anisotropy parameter β (eq. 20). When sufficiently close to the center, the anisotropy ratio is independent of the BH mass and the radius, and is determined solely by the initial Sérsic index m. The values of β for $m = 2.3$ and $m = 9$ obtained from equation (A6) are -0.313 and -0.306, respectively, and the corresponding values from Figure 8 are -0.285 and -0.247. The constant tangential anisotropy near the center contrasts with the situation for initial galaxies having analytical cores as described in Goodman & Binney (1984) and Quinlan et al. (1995): with analytic cores the initial DF is constant as $r \to 0$ so the ratio $\overline{v_r^2}/\overline{v_t^2}$ tends to $\frac{1}{2}$ and β tends to zero.

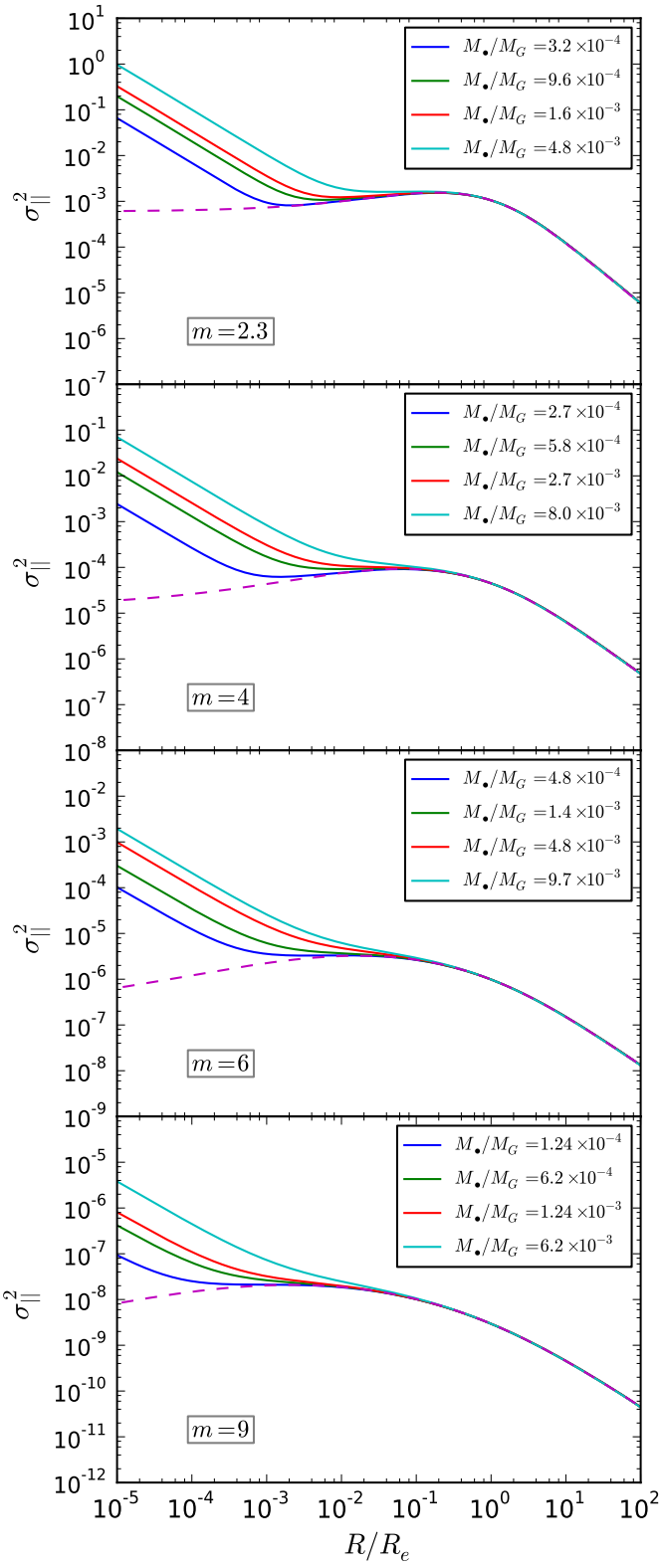

FIG. 9.— Line-of-sight velocity dispersion after the adiabatic growth of a BH in a galaxy with Sérsic index $m = 2.3$, $m = 4$, $m = 6$, $m = 9$. The dashed line is for the initial model without a BH.

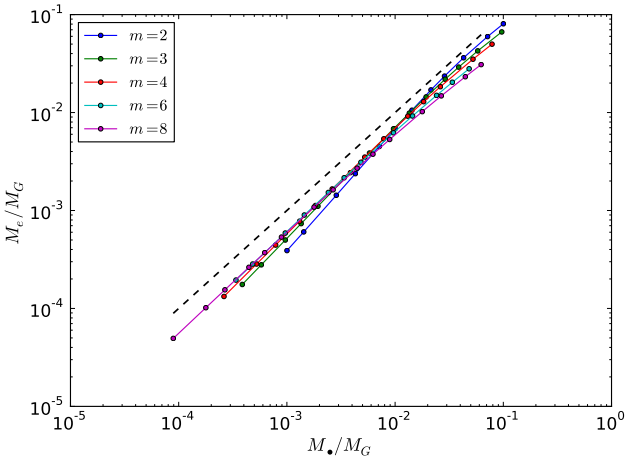

FIG. 10.— Excess mass vs. BH mass, both scaled to the mass of the galaxy. The dashed line is $M_\bullet = M_e$.

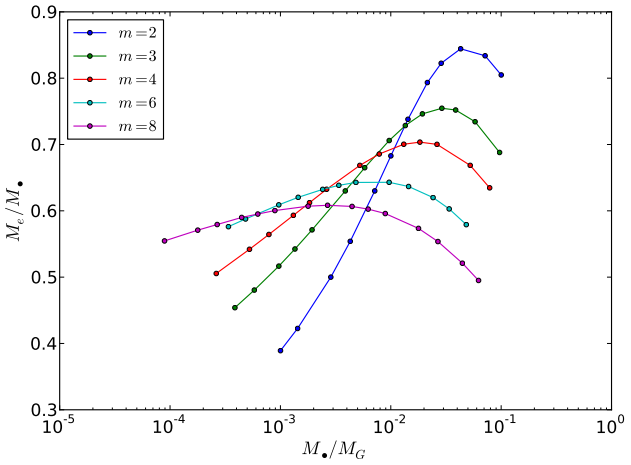

FIG. 11.— Ratio of the excess mass to the BH mass, as a function of BH mass. The abscissa is plotted on a log scale.

5.3. *Excess mass*

In Figure 10, we plot the excess mass (as defined in §4) with respect to the BH mass. We observe that the excess mass scales approximately linearly with the BH mass, although with some offset and curvature in the relation. To make these features more apparent we plot in Figure 11 the ratio of excess mass to BH mass as a function of the BH mass.

We see that the excess mass M_e is always smaller than the BH mass $M_\bullet$ for all values of the BH mass and all values of the Sérsic index m. There is a peak in the excess mass as a function of BH mass for all values of the Sérsic index, which occurs when the mass of the BH is between about 10^{-3} and $10^{-1.5}$ times the mass of the galaxy. The maximum of the ratio $M_e/M_\bullet$ increases as m decreases, consistent with the stronger visual appearance of the cusp in Figure 8 at smaller Sérsic index, but this maximum varies by less than a factor of two over a wide range of Sérsic indices.

The dependence of the ratio of the excess mass to BH mass shown in Figure 11 can be fitted to a cubic polynomial,

$$y = \frac{M_e}{M_\bullet} = a\,\chi^3 + b\,\chi^2 + c\,\chi + d\,; \quad \text{where} \quad \chi = \log\left(\frac{M_\bullet}{M_G}\right) \tag{25}$$

where the coefficients a, b, c and d are functions of m alone. Table 2 gives the fitted values of the coefficients of the cubic polynomial; the ratio of black hole mass to the galaxy mass at the maximum of $M_e/M_\bullet$ ($M_\bullet^{\max}/M_G$); and the maximum deviation of the fitting function $y_{\rm fit}$ from the numerically calculated values $y_{\rm num}$, that is, $\max(|y_{\rm fit} - y_{\rm num}|)$.

6. COMPARISON TO OBSERVATIONS

We now ask whether our results are consistent with observations of excess light in elliptical galaxies. Kormendy et al. (2009) estimate that the excess light is 0.3%–13% of the total light in the galaxy (median 2.3%); for comparison the typical ratio of BH mass to galaxy mass (in stars) is $M_\bullet/M_G \simeq 0.5\%$ (Kormendy & Ho 2013). Figure 11 then implies $M_e/M_\bullet \simeq 0.7$ so $M_e/M_G \simeq 0.3\%$–0.4%, at the lower end of the observed range. This result is consistent with the top panel of Figure 42 of Kormendy et al. (2009), which shows that $M_e/M_\bullet$ ranges between 1 and 50, with typical values around 10. In other words the adiabatic model correctly predicts that the excess mass should be roughly proportional to the galaxy or BH mass, but the predicted magnitude is too small by a factor 5–10. We conclude that the excess light in ellipticals does not arise from adiabatic growth of a central BH. This conclusion is consistent with the observation (Kormendy et al. 2009) that the excess light often has disky isophotes, suggesting that it formed via dissipative processes rather than by adiabatic ones—most likely late star formation due to gas that has collected in the central region of the galaxy (e.g., Hopkins et al. 2009).

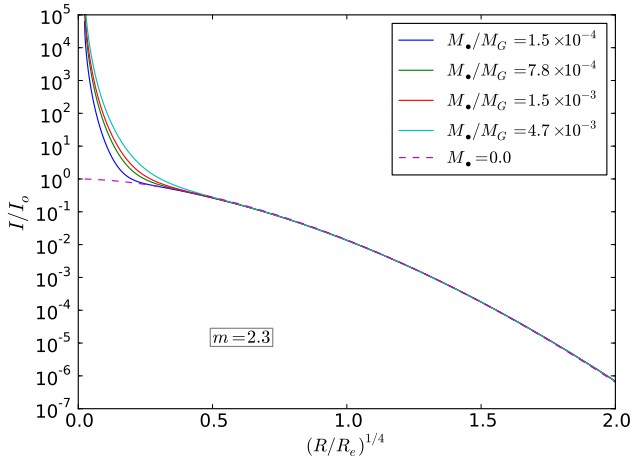

FIG. 12.— Surface-brightness profile of the galaxy with Sérsic index $m = 2.3$, plotted with respect to $(R/R_e)^{1/4}$. The dashed line is $M_\bullet = 0$.

Nuclei or nuclear star clusters are a different form of excess light at the centers of galaxies. Kormendy et al. (Section 9.7) make a distinction between the "excess light" in elliptical galaxies and the "nuclei" in spheroidal galaxies. In Figure 12 the surface brightness profile for a galaxy with Sérsic index $m = 2.3$ is plotted using the same $(R/R_e)^{1/4}$ abscissa as in Kormendy et al. Comparing this plot to Figures 25, 26, and 28 of that paper, we notice that the slope of the surface-brightness profile associated with nuclei in spheroidal galaxies, which is much steeper than the profile associated with excess light in ellipticals, is similar to what we obtain in the adiabatic-growth model. Moreover, the median light fraction of nuclei in spheroidal galaxies is 0.3% (Kormendy et al. 2009), much smaller than the fractional excess light in ellipticals and consistent with our model if the nuclei contain typical BHs with mass $M_\bullet/M_G \simeq 0.5\%$ (Kormendy & Ho 2013).

The observational relation between BHs and nuclear star clusters remains unclear. Côté et al. (2006) and Wehner & Harris (2006) have argued that nuclear star clusters and central BHs define a single smooth relationship between mass (of the cluster or BH) and galaxy luminosity, with clusters dominating at low luminosities and BHs at high luminosities. Kormendy et al. (2009) argue that this correlation is accidental, but our understanding of the correlation between BH masses and their host galaxy properties, particularly in low-luminosity and late-type galaxies, is too limited for a definite conclusion.

One attractive alternative to the formation of nuclear star clusters by the adiabatic growth of a BH is that the clusters form through in-spiral of globular clusters (Tremaine et al. 1975; Antonini 2013; Gnedin et al. 2014). In this case the BH could form before or after the bulk of the cluster formation.

TABLE 2
THE FITTED VALUES OF THE COEFFICIENTS a, b, c d IN EQUATION (25) AND $M_\bullet^{\max}/M_G$, THE BH MASS AT WHICH $M_e/M_\bullet$ IS LARGEST.

m	$-a$	$-b$	$-c$	d	$M_\bullet^{\max}/M_G$	$\max(\lvert y_{\rm fit} - y_{\rm num}\rvert)$
2	1.21×10^{-2}	1.84×10^{-1}	0.77	−0.140	5.21×10^{-2}	6.34×10^{-3}
3	5.25×10^{-3}	9.33×10^{-2}	0.46	0.0598	3.03×10^{-2}	5.183×10^{-3}
4	3.23×10^{-3}	6.36×10^{-2}	0.356	0.0897	1.76×10^{-2}	3.107×10^{-3}
5	2.47×10^{-3}	5.13×10^{-2}	0.312	0.0784	1.09×10^{-2}	1.115×10^{-3}
6	1.88×10^{-3}	4.14×10^{-2}	0.272	0.0810	6.78×10^{-3}	0.568×10^{-3}
7	1.39×10^{-3}	3.31×10^{-2}	0.236	0.0934	4.21×10^{-3}	0.761×10^{-3}
8	1.03×10^{-3}	2.64×10^{-2}	0.205	0.1070	2.65×10^{-3}	0.968×10^{-3}
9	9.19×10^{-4}	2.41×10^{-2}	0.194	0.0970	1.83×10^{-3}	0.574×10^{-3}

7. CONCLUSIONS

We have studied the effect of the adiabatic growth of a central black hole on the $R^{1/m}$ or Sérsic model of spherical galaxies, following the methods described by Young (1980). The black hole induces a surface-brightness cusp at the center of the galaxy, which can be described as "excess light" or "excess mass" above the inward extrapolation of the best-fit Sérsic profile for the outer galaxy. At the smallest radii the surface brightness is found to vary with radius as $I(R) \sim R^{-1.28}$ to $I(R) \sim R^{-1.32}$ for m varying from 2 to 9. Increasing the BH mass increases the strength of the cusp without changing the logarithmic slope near the center. The line-of-sight velocity dispersion is found to scale as $R^{-1/2}$, which is the expected behavior in a Keplerian potential; the anisotropy parameter β near the center is between -0.24 and -0.28 (tangential anisotropy).

We calculated the excess mass (defined as the mass interior to the radius on the sky where the initial and final surface densities were the same) for Sérsic models with varying indices m. The excess mass is generally between 0.4 and 0.85 times the black-hole mass.

If the typical black-hole mass is $\sim 0.5\%$ of the stellar mass in the galaxy, the excess mass produced by adiabatic contraction is $\sim$ 5–10 times smaller than the excess mass determined from Sérsic fits to the photometry of elliptical galaxies, but similar to the masses of nuclear star clusters in low-luminosity galaxies of all Hubble types. If black holes form by slow accretion of gas then adiabatic contraction may play an important role in determining the properties of nuclear star clusters.

This work was supported in part by NASA grant NNX14AM24G and NSF grant AST-1406166. Naveen Jingade(NJ) thanks S.Sridhar(RRI) for many fruitful discussions on this work and guiding through this project. NJ also thanks Raman Research Institute for hosting, where this work was carried out. NJ acknowledges the financial support of CSIR, India.

REFERENCES

Antonini, F. 2013, ApJ, 763, 62

Ciotti, L. 1991, A&A, 249, 99

Côté, P., Piatek, S., Ferrarese, L., et al. 2006, ApJS, 165, 57
Faber, S. M., Tremaine, S., Ajhar, E. A., et al. 1997, AJ, 114, 1771
Gnedin, O. Y., Ostriker, J. P., & Tremaine, S. 2014, ApJ, 785, 71
Gondolo, P., & Silk, J. 1999, Physical Review Letters, 83, 1719
Goodman, J., & Binney, J. 1984, MNRAS, 207, 511
Hopkins, P. F., Cox, T. J., Dutta, S. N., et al. 2009, ApJS, 181, 135
Kormendy, J., Fisher, D. B., Cornell, M. E., & Bender, R. 2009, ApJS, 182, 216
Kormendy, J., & Ho, L. C. 2013, ARA&A, 51, 511
MacMillan, J. D., & Henriksen, R. N. 2002, ApJ, 569, 83
Peebles, P. J. E. 1972, ApJ, 178, 371
Quinlan, G. D., Hernquist, L., & Sigurdsson, S. 1995, ApJ, 440, 554
Sérsic, J. L. 1963, Boletin de la Asociacion Argentina de Astronomia La Plata Argentina, 6, 41
Sérsic, J. L. 1968, Atlas de galaxias australes (Córdoba: Observatorio Astronomico, Universidad Nacional de Córdoba)
Tremaine, S. D., Ostriker, J. P., & Spitzer, Jr., L. 1975, ApJ, 196, 407
Wehner, E. H., & Harris, W. E. 2006, ApJL, 644, L17
Young, P. 1980, ApJ, 242, 1232

8. APPENDIX

The goal of this Appendix is to determine the velocity anisotropy near the center of the cusp formed by the adiabatic growth of a central BH.

The density for a spherically symmetric Sérsic profile of index m can be approximated near the center as (eq. 5):

$$\rho_m(s) = \rho_o\, s^{-\gamma} \quad \text{where} \quad \gamma = (m-1)/m\,, \tag{A1}$$

and the corresponding potential is

$$\Phi_m(s) - \Phi_m(0) = \frac{\rho_o}{(3-\gamma)(2-\gamma)} s^{2-\gamma} = \phi_o\, s^{2-\gamma}\,. \tag{A2}$$

The phase-space DF for the above density and potential pair is given by equation (13):

$$f_m(E) \sim [E - \Phi_m(0)]^{-\alpha}\,, \qquad \alpha = \frac{6-\gamma}{2(2-\gamma)} = \frac{5m+1}{2(m+1)}. \tag{A3}$$

An approximate expression for the radial action (Gondolo & Silk 1999) accurate to 8% for all $m > 1$ is

$$I_r(E,L) = \frac{2\pi}{d}\left\{ -\frac{L}{\lambda} + \sqrt{2\,\phi_o}\left[\frac{E-\Phi_m(0)}{\phi_o}\right]^{(4-\gamma)/(4-2\gamma)}\right\}, \tag{A4}$$

where

$$\lambda = \frac{2^{1/(2-\gamma)}(2-\gamma)^{1/2}}{(4-\gamma)^{(4-\gamma)/(4-2\gamma)}}; \qquad d = \pi\frac{(2-\gamma)}{B\left[1/(2-\gamma), \frac{3}{2}\right]}.$$

Once the black hole grows adiabatically, the galaxy potential at the center is approximately Keplerian. The radial action is now given by $I_r^*(E^*, L) = 2\pi\big(M_\bullet/\sqrt{-2\,E^*} - L\big)$. The final DF $f^*(E^*, L)$ is obtained by solving $I_r(E,L) = I_r^*(E^*,L)$ for E as a function of E^* and L. Using the equation $E^* = \frac{1}{2}v^2 - M_\bullet/s$ and $L = s\,v_t$ to eliminate E^* and L in favor of the total and tangential speeds v and v_t, we find that the dependence of the final DF on velocity at a given radius can be written as

$$f^* \sim \left[\left(\frac{1}{\lambda d} - 1\right) x \sin\psi + \frac{x_m^2}{2\sqrt{x_m^2 - x^2}}\right]^{-\delta}, \tag{A5}$$

where

$$\delta = \frac{6-\gamma}{4-\gamma} \quad ; \quad x = sv \quad ; \quad x_m = \sqrt{2M_\bullet\, s} \quad ; \quad v_t = v\sin\psi\,.$$

The quantities x and x_m are defined following Goodman & Binney (1984).

Multiplying f^* by v_r^2 and v_t^2 and integrating over all velocities we obtain the ratio of velocity dispersions and the anisotropy parameter β:

$$\frac{\overline{v_r^2}}{\overline{v_t^2}} = \frac{1}{2(1-\beta)} = \frac{\displaystyle\int_0^1 \mathrm{d}y\, y^4 \int_0^\pi \mathrm{d}\psi\, \sin\psi\cos^2\psi \left[\left(\frac{1}{\lambda d} - 1\right) y\sin\psi + \frac{1}{2\sqrt{1-y^2}}\right]^{-\delta}}{\displaystyle\int_0^1 \mathrm{d}y\, y^4 \int_0^\pi \mathrm{d}\psi\, \sin^3\psi \left[\left(\frac{1}{\lambda d} - 1\right) y\sin\psi + \frac{1}{2\sqrt{1-y^2}}\right]^{-\delta}}, \tag{A6}$$

where $y = x/x_m$. The only approximation in deriving this result is the approximate form for the radial action, equation (A4). The quadratures are straightforward to evaluate numerically.